Published in final edited form as:

Immunity. 2010 October 29; 33(4): 583–596. doi:10.1016/j.immuni.2010.09.010.

The Rab11a GTPase Controls Toll-like Receptor 4-Induced Activation of Interferon Regulatory Factor-3 on Phagosomes

Harald Husebye[1,9], **Marie Hjelmseth Aune**[1,9], **Jørgen Stenvik**[1,9], **Eivind Samstad**[1], **Frode Skjeldal**[3], **Øyvind Halaas**[1], **Nadra J. Nilsen**[1], **Harald Stenmark**[1,4], **Eicke Latz**[1,5], **Egil Lien**[1,6], **Tom Eirik Mollnes**[2], **Oddmund Bakke**[3,7], **Terje Espevik**[1,8,*]

[1]Norwegian University of Science and Technology, Department of Cancer Research and Molecular Medicine, N-7489 Trondheim, Norway

[2]Institute of Immunology, Rikshospitalet University Hospital, University of Oslo, N-0027 Oslo, Norway

[3]Department of Molecular Biosciences, Centre for Immune Regulation, University of Oslo, N-0316 Oslo, Norway

[4]Department of Biochemistry, Institute for Cancer Research, The Norwegian Radium Hospital, Montebello, N-0310 Oslo, Norway

[5]Institute of Innate Immunity, Biomedical Center, University of Bonn, Sigmund-Freud-Str. 25, 53127 Bonn, Germany

[6]Division of Infectious Diseases and Immunology, University of Massachusetts Medical School, Worcester, MA 01605, USA

[7]The Gade Institute, University of Bergen, 5021 Bergen, Norway

[8]St. Olavs Hospital, N-7489 Trondheim, Norway

[9]These authors contributed equally to this work

SUMMARY

Toll-like receptor 4 (TLR4) is indispensable for recognition of Gram-negative bacteria. We described a trafficking pathway for TLR4 from the endocytic recycling compartment (ERC) to *E. coli* phagosomes. We found a prominent colocalization between TLR4 and the small GTPase Rab11a in the ERC, and Rab11a was involved in the recruitment of TLR4 to phagosomes in a process requiring TLR4 signaling. Also, Toll-receptor-associated molecule (TRAM) and interferon regulatory factor-3 (IRF3) localized to *E. coli* phagosomes and internalization of *E. coli* was required for a robust interferon-β induction. Suppression of Rab11a reduced TLR4 in the ERC and on phagosomes leading to inhibition of the IRF3 signaling pathway induced by *E. coli,* whereas activation of the transcription factor NF-κB was unaffected. Moreover, Rab11a silencing reduced the amount of TRAM on phagosomes. Thus, Rab11a is an important regulator

*Correspondence: terje.espevik@ntnu.no.

SUPPLEMENTAL INFORMATION

Supplemental Information includes Supplemental Experimental Procedures, seven figures, and one movie and can be found with this article online at doi:10.1016/j.immuni.2010.09.010.

of TLR4 and TRAM transport to *E. coli* phagosomes thereby controlling IRF3 activation from this compartment.

INTRODUCTION

Toll-like receptor 4 (TLR4) has an essential role in host defense against Gram-negative bacteria (Montminy et al., 2006; Poltorak et al., 1998). The signaling receptor for lipopolysaccharide (LPS) is TLR4 in complex with myeloid differentiation factor 2 (MD-2), which receives LPS from CD14 (Gioannini et al., 2004). The TLR4 signaling cascade is mediated through the Toll and Interleukin-1 receptor (TIR)-adaptors myeloid differentiation factor 88 (MyD88), TIR-domain-containing adaptor protein (TIRAP, also known as MyD88 adaptor-like protein), Toll-receptor-associated activator of interferon (TRIF), Toll-receptor-associated molecule (TRAM), and Sterile α- and armadillo-motif containing protein (SARM) (O'Neill and Bowie, 2007). TLR4 signaling proceeds through a MyD88-dependent and MyD88-independent pathway. The MyD88-dependent pathway rapidly activates NF-κB and mainly takes place at the plasma membrane (Kagan and Medzhitov, 2006; Latz et al., 2002), whereas the MyD88-indenpendent pathway activates interferon regulatory factor-3 (IRF3) and occurs at early endosomes (Halaas et al., 2007; Kagan et al., 2008). Systemic infections with Gram-negative bacteria may lead to septic shock, multiorgan failure, and death (Waage et al., 1989). Therefore, fine-tuning of the TLR4 response is of essential importance in regulating inflammatory reactions against Gram-negative bacteria.

Macrophages and neutrophils eliminate invading pathogens and foreign particles by first ingesting them into a plasma membrane-derived intracellular vacuole termed the phagosome. The formation of the phagosome and phagocytosis per se is a receptor-mediated and actin-dependent process. The resulting phagosome undergoes a series of fusion and fission events through a sequence that resembles the endocytic pathway, referred to as phagosomal maturation (Flannagan et al., 2009). Although soluble LPS is a primary inducer of host responses against Gram-negative bacteria, LPS on the bacterial surface contributes to both phagocytosis and TLR4 signaling. This is demonstrated by recent data showing that MD-2 acts as an opsonin for Gram-negative bacteria (Jain et al., 2008; Tissières et al., 2008). Having MD-2 on the surface of Gram-negative bacteria is likely to result in binding to and aggregation of TLR4 on the envelope that forms during phagocytosis. A consequence of TLR4 aggregation is potent signaling events that can be demonstrated as high tumor necrosis factor (TNF) production in human PBMC (Latz et al., 2002).

Rab proteins are small guanosine triphosphatases (GTPases) that have key roles in membrane transport and fusion (Jordens et al., 2005). Rab4 is a main regulator of exocytosis and rapid recycling of membrane receptors whereas Rab5 and Rab7 control early endocytic transport and late endocytic membrane traffic, respectively. Thus, both Rab5 and Rab7 have essential functions in phagosome maturation (Kinchen and Ravichandran, 2008). The Rab11 subfamily consists of three isoforms— Rab11a, Rab11b, and Rab25. Rab11a and Rab11b are ubiquitously expressed, whereas Rab25 expression is restricted to epithelial cells (Goldenring et al., 1993; Lapierre et al., 2003). Rab11 proteins regulate the "slow" recycling of the transferrin receptor to the plasma membrane and Rab11 is highly concentrated in the

perinuclear endocytic recycling compartment (ERC) (Ullrich et al., 1996). Like all GTPases of the Ras family, Rab11 functions as a molecular switch. Rabs associate with membranes in the guanosine diphosphate (GDP)-bound form and switch to a GTP-bound conformation in a reaction catalyzed by a GEF (guanine-nucleotide-exchange factor). In the active GTP-bound state, they interact with downstream effector proteins that coordinate vesicle formation, vesicle and organelle motility, and the tethering of vesicles to their target compartment (Zerial and McBride, 2001). Rab11 binds to Rab11 family interacting protein 2 (FIP2) that recruits the actin motor MyoVb that mediates transports of cargo along actin filaments (Jordens et al., 2005; Wei et al., 2009). Of interest, Rab11 has been reported to be associated with phagosomes (Cox et al., 2000) and to be involved in the intracellular transport of pro-TNF from the Golgi complex to the phagocytic cup (Murray et al., 2005). TLR2 is recruited to macrophage phagosomes containing zymosan particles and *S. aureus* (Ip et al., 2008; Nilsen et al., 2004) as well as to immunoglobulin-G (IgG)-coated erythrocytes (Ozinsky et al., 2000). Also, TLR4 accumulates at the phagocytic cup that develops around *E. coli* in HEK293 cells overexpressing TLR4, CD14, and MD-2 (Espevik et al., 2003). However, no information exists on possible functions of Rab11 in cytokine responses and whether Rab11 controls trafficking of TLR4 to phagosomes containing Gram-negative bacteria.

We found that TLR4 strongly colocalized with Rab11a, in particular in the ERC. Our data demonstrate that Rab11a controls trafficking of TLR4 in and out of ERC and that Rab11a is involved in transport of TLR4 to the *E. coli* phagosome. Furthermore, we have documented that phagocytosis of *E. coli* is required for interferon-β (IFN-β) production and that Rab11a is a specific regulator of TLR4-induced IRF3 activation and IFN-β production.

RESULTS

Perinuclear TLR4 Is Located in the Rab11a$^+$ ERC

Earlier reports suggest that the large perinuclear pool of TLR4 is localized to the Golgi apparatus (Hornef et al., 2002; Latz et al., 2002; Uronen-Hansson et al., 2004). However, because the Rab11-positive perinuclear endocytic recycling compartment (ERC) is in close vicinity to the Golgi apparatus (Jones et al., 2006; Saraste and Goud, 2007), we wanted to carefully analyze in 3D the spatial localization of TLR4 in relation to markers for Golgi and ERC. HEK293 cells stably expressing TLR4 fused to yellow fluorescent protein ($TLR4^{YFP}$) were transfected with a trans-medial Golgi marker β−1,4-galactosyl transferase fused to cyan fluorescent protein (β−1,4-GT^{CFP}) and subjected to optical sectioning. As can be seen in Figure 1A, there is only a partial overlap between TLR4 and β−1,4-GT^{CFP} that identifies the trans-medial Golgi as a ring structure (Misaki et al., 2007). The highest TLR4 intensity was found inside the center of the Golgi ring, which is clearly visualized in both planar and orthographic projections (Figure 1A). We next examined whether the high amounts of TLR4 expression inside the Golgi ring represented the Rab11a-positive ERC. HEK293-$TLR4^{YFP}$ cells were labeled with Rab11a antibodies and examined by confocal microscopy. The results demonstrate that there is a strong colocalization of TLR4 and endogenous Rab11a (Figure 1B) suggesting that TLR4 accumulates in the ERC. Similar data were also obtained when $Rab11a^{CFP}$ was expressed in the HEK293-$TLR4^{YFP}$ cells (Figure 1C; Figure S1A available online). Transfection of a dominant-negative GDP-bound

version of Rab11a (Rab11aSN^{GFP}) into HEK293-TLR4^{Cherry} caused a redistribution of TLR4 from ERC to endosomes close to the plasma membrane, whereas the constitutively active GTP variant of Rab11a (Rab11aQL^{GFP}) sequestered TLR4 in numerous vesicles that were positive for Rab11aQL^{GFP} (Figures 1D and 1E). Thus, Rab11a has an essential role in localization of TLR4 to the ERC. In addition to the marked accumulation in ERC, Rab11a was also expressed on tubular structures throughout the cell and on the limiting membrane of enlarged endosomes where it frequently colocalized with TLR4 (Figure S1A). Three-dimensional reconstruction of optical sections revealed that TLR4 and Rab11a were colocalized inside the *cis*-Golgi ring in HEK293-TLR4^{YFP} cells (Figure 1C; Figure S1B). Because TLR4^{YFP} is overexpressed in HEK293 cells, we wanted to confirm the above data in human monocytes. Relatively low amounts of TLR4 are found on the plasma membrane of human monocytes, whereas considerable amounts of TLR4 are detected in intracellular compartments (Latz et al., 2002). By using antibodies against a trans-medial Golgi marker and TLR4, we found that TLR4 was concentrated inside the Golgi ring also in monocytes (Figure 2A). Furthermore, TLR4 and Rab11a displayed a marked colocalization in human monocytes, particularly in the perinuclear ERC (Figure 2B). Rab11 has been reported to interact with G protein-coupled receptors (Parent et al., 2009). Therefore, we examined whether TLR4 and Rab11a could physically interact. Coimmunoprecipitation experiments were carried out in HEK293 cells stably expressing HA-tagged TLR4 and cotransfected with Flag-tagged Rab11a; however, no association between TLR4 and Rab11a was observed (Figure S2). These data demonstrate that TLR4 accumulates in the Ra11a^{+} ERC that is located inside the Golgi ring.

TLR4 and Rab11a Accumulate around Phagocytosed *E. coli* but Not around *S. aureus*

Because TLR4 and Rab11a showed prominent colocalization, we wanted to investigate the role for Rab11a in trafficking of TLR4 to phagosomes containing *E. coli.* Human monocytes were incubated with pHrodo (a pH-sensitive, rhodamine-based dye)-labeled *E. coli* or *S. aureus* bioparticles before they were fixed and stained for TLR4. A strong accumulation of TLR4 around *E. coli* phagosomes was observed (Figure 3A). In early phases of phagosome formation, TLR4 seemed to be recruited to the phagocytic cup from intracellular vesicles whereas later in the phagocytosis process, TLR4 was found around the *E. coli* particle (Figures S3A and S3B). Recruitment of TLR4 to *E. coli* phagosomes was also apparent when live *E. coli*^{YFP} was used (data not shown). No accumulation of TLR4 was observed around *S. aureus* phagosomes (Figure 3B), suggesting that this phenomenon is specific for Gram-negative bacteria. We next investigated whether Rab11a was recruited to phagosomes. As seen for TLR4, Rab11a showed a clear accumulation around *E. coli*- but not *S. aureus*-containing phagosomes in human monocytes (Figures 3C and 3D).

Phagocytosis of *E. coli* Reduces TLR4 and Rab11a in the ERC

The effect of a challenge with *E. coli* on the TLR4 pool in ERC was investigated. In order to obtain a nonbiased and accurate measurement of TLR4 intensities, optical sections of monocytes were obtained and the amounts of TLR4 in the ERC were estimated by measuring the sum of voxel intensity of each ERC via 3D image analysis. The median TLR4 voxel intensity in the ERC was estimated in monocytes with and without added bacteria for 15 min (Figure 4A). A significant reduction of TLR4 in the ERC was observed when *E. coli*

was added. Also, the voxel intensity of Rab11a in the ERC was reduced after addition of *E. coli* for 15 min (Figure 4B). These data suggest that addition of *E. coli* is emptying the ERC for both TLR4 and Rab11a.

TLR4 and Rab11a on Phagosomes Are Affected by *E.coli* Incubation Time

Next, we monitored the amount of TLR4 and Rab11a on phagosomes at different maturation states. In a time kinetic study, monocytes were exposed to *E. coli* for 15 min, for 30 min, and for 30 min followed by an additional 30 min in medium ("pulse-chase"). The median TLR4 voxel intensity on *E. coli* phagosomes was measured by 3D image analysis for each of the three time points (Figure 4C). This revealed that the amount of TLR4 on phagosomes increased as a function of *E. coli* incubation time. Worth noting is that the 30+30 min pulse-chase resulted in significant increase of TLR4 on phagosomes compared to the 30 min exposure (Figure 4C). This result suggests that TLR4 is recruited to the maturing phagosome by mechanisms that involve trafficking of TLR4 mainly from intracellular compartments. We also wanted to compare the kinetics of TLR4 and Rab11a accumulation on *E. coli* phagosomes. In contrast to TLR4, the amount of Rab11a was highest around *E. coli* after 15 min followed by a gradual decrease on maturing phagosomes (Figure 4D). The dynamics of Rab11a recruitment to *E. coli* was further studied by confocal live cell imaging of immortalized murine macrophages stably expressing $Rab11a^{GFP}$ (Figures S4A–S4C and Movie S1). Time series images of an *E. coli* entering a macrophage revealed that $Rab11a^{GFP}$ rapidly trafficked by small vesicles and tubules that seemed to fuse with the developing phagosome (Figure S4A). After 35 min of *E. coli* incubation, a considerable amount of $Rab11a^{GFP}$ was observed on the phagosome and processes resembling both fusion and fission events of $Rab11a^{GFP}$-positive vesicles on phagosomes were observed (Figures S4B and S4C). The observed reduction in the Rab11a on maturing phagosomes (Figure 4D) may thus be due to a time-dependent increase in the fission-fusion ratio of Rab11a vesicles associated with *E. coli* phagosomes.

Accumulation of TLR4 around Phagosomes Requires TLR4 Signaling and Results in Strong IFN-β Induction

We next wanted to see whether Gram-negative bacteria other than *E. coli* induced mobilization of TLR4 to the phagosomes, and whether this phenomenon required an LPS type that activates TLR4. *Y. pestis* grown at 37°C produces a tetraacylated LPS that poorly stimulates TLR4 whereas *Y. pestis* grown at 26°C produces a hexaacylated LPS with high TLR4-stimulating properties (Montminy et al., 2006). The two *Y. pestis* variants were labeled with CFP, heat-killed bacteria were added to monocytes, and the median voxel intensity of TLR4 around *Y. pestis* phagosomes was quantified with 3D image analysis. As can be seen from Figure 5A, *Y. pestis* grown at 37°C was a poor inducer of TLR4 recruitment to the phagosomes, whereas TLR4 was strongly recruited to phagososmes with *Y. pestis* grown at 26°C. This result suggests that phagosomal TLR4 accumulation requires Gram-negative bacteria that produce a TLR4-stimulating LPS.

A likely consequence of TLR4 accumulation at the phagosomes is that TLR4 signaling occurs from this compartment. In order to initiate TLR4 signaling from the phagosomes, adaptor molecules must also be recruited. TRAM interacts with TRIF and is required for

IRF3 activation. MyD88 is the universal adaptor for TLRs that activates NF-κB, c-Jun kinase, and p38 mitogen-activated protein kinase (O'Neill and Bowie, 2007). Therefore, we wanted to examine whether the adaptor molecules TRAM and MyD88 were recruited to phagosomes containing *E. coli*. We found that both TRAM and MyD88 strongly accumulated around phagosomes (Figure 5B; Figures S5A, S5B, and S5E). In line with the TRAM observation, we also detected prominent recruitment of IRF3 to *E. coli* phagosomes (Figure 5C; Figure S5C). These data suggest that *E. coli* initiates powerful signaling from this compartment.

Having described that TLR4 accumulation on phagosomes is associated with TRAM, MyD88, and IRF3 recruitments, we next wanted to address the involvement of actin filaments, Golgi, and dynamin GTPase in the recruitment of TLR4 to phagosomes. Inhibition of actin polymerization with cytochalasin D (cyto D) reduced the number of internalized bacteria by approximately 65% (Figure S6C) as well as the recruitment of TLR4 to *E. coli* phagosomes (Figure 5D). In contrast, brefeldin A, which inhibits ADP-ribosylation factor 1 (Arf 1) leading to retraction of Golgi membranes back into the ER, did not influence the amount of TLR4 associated with *E. coli* phagosomes (Figure 5E). It has previously been reported that TLR4 is internalized from the plasma membrane by a dynamin-dependent process (Husebye et al., 2006; Kagan et al., 2008). Pulse chase experiments with *E. coli* showed that TLR4 was almost doubled during the 30+30 min chase experiment (Figure 4C), so we added the dynamin inhibitor Dynasore (Kagan et al., 2008) during the last 30 min of the pulse-chase to see whether this treatment inhibited TLR4 recruitment to phagosomes. Quantitative analyses of phagosomal TLR4 revealed no inhibitory effect of Dynasore. In fact, Dynasore treatment weakly increased the TLR4 amounts (Figure 5F). Dynasore treatment inhibited the LPS-induced IFN-β mRNA by approximately 70%, whereas the LPS-induced TNF response was inhibited by only 30% (Figure S5F). The *E. coli*-induced IFN-β and TNF responses were only weakly inhibited (15%–18%) when Dynasore was added with the last 30 min chase (Figure S5F). These results suggest that dynamin is not involved in TLR4 transport to phagosomes and that the plasma membrane is not the main source of phagosomal TLR4.

Because of the pronounced accumulation of TLR4, TRAM, and IRF3 to *E. coli* phagosomes, we wanted to address the involvement of phagocytosis in cytokine production. In the first set of experiments, we compared the potency of *E. coli* and LPS from *E. coli* in inducing IFN-β and TNF mRNA. We found that the maximum IFN-β response induced by *E. coli* was around 700% higher compared to the maximum IFN-β response induced by LPS. In contrast, the TNF mRNA was only around 60% higher for *E. coli* compared to LPS (Figures 6A and 6B). The robust IFN-β response obtained with *E. coli* seemed to be specific for Gram-negative bacteria as shown by the fact that *S. aureus* did not induce detectable IFN-β under the same experimental conditions (data not shown). Furthermore, the potent IFN-β induction required LPS in the bacteria because a *N. meningitidis* mutant without LPS induced minimal IFN-β production compared to the wild-type *N. meningitides* (Figure S6A). Thus, *E. coli* is far more potent in inducing IFN-β than LPS, whereas a considerable lesser difference between *E. coli* and LPS is seen for the TNF response. Because opsonization of bacteria increases phagocytosis (Johnston et al., 1969), we used serumopsonized and nonopsonized *E. coli* and compared the induction of IFN-β and TNF.

We observed that opsonization of *E. coli* increased the IFN-β production by 300%, whereas opsonization increased the TNF response by only 20%. The fact that opsonization clearly increases the number of internalized *E. coli* in monocytes was verified by flow cytometry (data not shown). Another way to inhibit phagocytosis is to use cyto D. We found that 2 μM cyto D inhibited *E. coli*-induced IFN-β by 53% whereas the TNF response was reduced by only 17%. According to the dose response curve in Figure 6A, a 10-fold (90%) reduction in *E. coli* concentration (from 10^7/ml to 10^6/ml) corresponded to a 50%–60% reduction in the IFN-β mRNA. If we assume a linear relationship between added *E. coli* to monocytes and internalized *E. coli*, a 90% reduction in phagocytosed *E. coli* would result in a 50%–60% inhibition of IFN-β mRNA. Because cyto D treatment inhibited the IFN-β response and *E. coli* uptake by 53% and 65%, respectively, it is likely that the reduction in IFN-β mRNA after cyto D treatment is an effect mainly resulting from reduced uptake, but also from a contribution from failure to deliver TLR4 to the phagosome membrane. Addition of cyto D had minimal effect on LPS-induced IFN-β and TNF (Figures 6C and 6D). Together these data clearly demonstrate a selective and important role of *E. coli* phagocytosis in the IFN-β response.

Suppression of Rab11a Results in Emptying of TLR4 from the ERC and Reduction of TLR4 around Phagosomes

To investigate the role of Rab11a in trafficking of TLR4 from the ERC to phagosomes, we performed experiments where we specifically silenced Rab11a. Consequently, human monocytes and HEK293-TLR4^{YFP} cells were treated with Rab11a siRNA or nonsilencing control RNA (NS RNA). The silencing was verified by immunoblotting. The Rab11a amount was reduced by approximately 90% in HEK293-TLR4^{YFP} cells and 60% in monocytes when quantified with a Kodak Imager (Figure 6E). Suppression of Rab11a minimally affected the Rab7a in monocytes and HEK293-TLR4^{YFP} cells (Figure 6E). Also, Rab11a siRNA treatment reduced the mRNA for Rab11a by approximately 60% in monocytes, whereas the Rab11b mRNA was unaffected (Figure S6C). After establishing the conditions for proper Rab11a silencing, we examined whether the intensity of TLR4 in ERC was affected by this treatment. We observed a significant reduction in TLR4 voxel intensity in the ERC in monocytes when the Rab11a was reduced (Figure S6E). This observation was also verified in HEK293-TLR4^{YFP} cells where the intense accumulation of TLR4 in the ERC disappeared completely in cells treated with Rab11a siRNA (Figure 6F). Additional experiments via flow cytometry showed that Rab11a suppression only minimally affected the total amount of TLR4 in HEK293-TLR4^{YFP} cells (data not shown). Furthermore, immunoblotting of TLR4 in monocytes did not reveal a reduction in total TLR4 amounts in Rab11a-silenced cells (data not shown). We did not observe a reduction in the number of phagocytosed bacteria in monocytes treated with Rab11a siRNA (Figure S6D). The amount of phagocytosed bacteria in Rab11a-silenced monocytes was quantified both by manual counting from the 3D data obtained from the confocal microscope and by flow cytometry (data not shown).

We next addressed the role of Rab11a in trafficking of TLR4 to phagosomes. The amount of TLR4 around *E. coli* was determined in monocytes treated with Rab11a siRNA and control oligo. The result from this experiment revealed an approximately 50% reduction in TLR4

voxel intensity around *E. coli* in Rab11 asilenced cells compared to the control siRNA-treated cells (Figure 6G). The reduced amount of TLR4 on phagosomes was observed at both 15 min and 30 min after addition of *E. coli.* In addition, we observed that recruitment of TRAM to *E. coli* phagosomes was reduced by approximately 50% in monocytes treated with Rab11a siRNA (Figure 6H). In parallel experiments we did not observe reduction in recruitment of MyD88 to *E. coli* phagosomes in monocytes treated with Rab11a siRNA (Figure S6G). Taken together, our results show that Rab11a controls trafficking of both TLR4 and TRAM to the *E. coli* phagosome most probably by mechanisms affecting the transport of TLR4 and TRAM vesicles in and out of the ERC.

Suppression of Rab11a Selectively Inhibits *E. coli*-Induced IRF3 Activation and IFN-β Production

TLR4 activates MyD88- and TRAM-TRIF-dependent signaling pathways from the plasma membrane and the endosome, respectively. Therefore, we wanted to address whether Rab11a differentially affected these two pathways in monocytes and in HEK293-TLR4 cells. We first examined the effect of Rab11a siRNA treatment on IRF3 phosporylation in monocytes stimulated with *E. coli* and LPS. As can be seen from Figures 7A and 7B, Rab11a silencing resulted in an almost complete inhibition of IRF3 phosphorylation induced by both *E. coli* and LPS. We next explored whether activation of NF-κB was affected by Rab11a siRNA treatment. NF-κB activation was measured as degradation of IκB-α after addition of *E. coli.* Suppression of Rab11a did not affect IκB-α degradation either in monocytes (Figure 7C) or in HEK293-TLR4^{YFP} cells expressing MD-2 and CD14 (Figure 7D). This result suggests that NF-κB activation is not controlled by Rab11a. The role of Rab11a in IRF3 activation was confirmed via IRF3 and NF-κB reporter assays. The Gal4-IRF3 fusion protein and the endothelial adhesion molecule-luciferase (ELAM-luc) reporter were used to measure IRF3 and NF-κB activation, respectively, in HEK293-TLR4^{Cherry} cells expressing MD-2 and CD14. Rab11a knockdown gave a marked inhibition of *E. coli*- and LPS-induced signaling to IRF3, whereas NF-κB activation was unaffected (Figures 7E and 7F). Additional support for the selectivity of Rab11a in controlling *E. coli*-induced signaling to IRF3 was obtained by measuring nuclear translocation of IRF3 and NF-κB subunit p65 in monocytes. Suppressing the Rab11a led to a significant inhibition of IRF3 that translocated to the nucleus in response to *E. coli* (Figure 7G). In contrast, p65 translocation was not inhibited by the siRNA treatment (Figure 7H). In fact, Rab11a suppression resulted in a weak increase in p65 translocation after 30 min with *E. coli.* In line with these findings, treatment of monocytes with Rab11a siRNA led to a 65% inhibition of *E. coli*-induced IFN-β mRNA production at both 30 and 60 min of stimulation, whereas the TNF mRNA amounts were unaffected (Figures 7I and 7J). When *E. coli* and LPS responses were compared, it became apparent that Rab11a siRNA treatment selectively inhibited LPS-induced IFN-β production that was comparable to *E. coli* (Figure S7).

In summary, our results demonstrate that Rab11a has an essential function in localizing TLR4 to phagosomes and controlling IRF3 activation and IFN-β production in response to *E. coli* and also LPS.

DISCUSSION

Phagocytosis and concomitant induction of proinflammatory cytokines are two instrumental events of an innate immune response against bacteria. In this study we describe an unexpected route for TLR4 recruitment to the *E. coli* phagosome by recycling mechanisms involving Rab11a. This conclusion is based on our observations that TLR4 is strongly expressed in the Rab11a-positive ERC that is localized inside the Golgi ring. Furthermore, TLR4 and Rab11a were recruited to *E. coli* phagosomes and suppression of Rab11a significantly inhibited the amount of TLR4 and TRAM around the phagosomes as well as signaling to IRF3 and IFN-β induction. The rapid accumulation of TLR4 was not observed in response to Gram-positive bacteria *S. aureus* or against *Y. pestis* with a nonstimulating LPS, suggesting that recruitment of TLR4 to *E. coli* requires TLR4 signaling.

Phagocytosis of *E. coli* and recruitment of TLR4, TRAM, and IRF3 to the phagosome implicate a strong type I IFN response from the vacuole. Indeed, our data have demonstrated that phagocytosis of *E. coli* is required for a robust IFN-β response, whereas phagocytosis is minimally involved in the TNF response. Recently, Ip and coworkers (Ip et al., 2010) reported that phagocytosis is necessary for MyD88-dependent TNF production induced by Gram-positive bacteria although this is not the case for Gram-negative bacteria. They also showed that phagosome acidification was needed to initiate the TNF production induced by *S. aureus.* We found that lysosomal inhibitors like Bafilomycin A1 and NH_4Cl inhibited neither IRF3 phosporylation nor the IFN-β response induced by *E. coli* (data not shown), suggesting that LPS in the bacterium is already accessible for TLR4 sensing without the need for enzymatic processing in the phagosome. The IRF3 pathway can be activated by LPS in the absence of phagosomes; however, because *E. coli* is much more potent in inducing IFN-β compared to LPS, it is likely that internalization of the bacteria is the prevailing pathway for IFN-β production during *E. coli* infections.

Our data have demonstrated that Rab11a mediates trafficking of TLR4 from the ERC to *E. coli* phagosomes. We suggest that TLR4 recycling to phagosomes from the ERC may occur constitutively without the need for TLR4 signaling. This would be in accord with the fact that Rab11 regulates the constitutive recycling of transferrin receptors through the ERC (Ullrich et al., 1996). When TLR4 encounters a phagosome with *E. coli*, TLR4 is activated for signaling, which may lead to formation of stable receptor complexes and development of signaling platforms resulting in TLR4 accumulation. This statement is supported by our observations that TRAM, MyD88, and IRF3 are all present on *E. coli* phagosomes. Moreover, as the maturation proceeds, TLR4 may then be internalized into the lumen of intermediate and late phagosomes by mechanisms similar to the described sorting of the LPS receptor complex to late endosomes and lysosomes (Husebye et al., 2006; Kobayashi et al., 2006).

Kagan and coworkers have suggested that TLR4 is recruited to the endosome from the plasma membrane and that TRAM-TRIF displaces MyD88 on the endosome as the TLR4 signaling switches from a MyD88- to a TRAM-TRIF-dependent pathway. Our data have suggested a different model where Rab11a mediates recruitment of TLR4 from the ERC to the *E. coli* phagosome. Our model is supported by data showing that TLR4 is strongly

expressed in the ERC compared to the plasma membrane, silencing of Rab11a results in a marked reduction of TLR4 in the ERC and also around *E. coli* vacuoles, and the amount of TLR4 on phagosomes increases during phagosomal maturation. Furthermore, inhibition of dynamin with Dynasore inhibits internalization of TLR4 (Kagan et al., 2008); however, Dynasore did not inhibit TLR4 recruitment to *E. coli* phagosomes. Thus, our data suggest that TLR4 is recruited from the ERC to phagosomes allowing for TRIF signaling to occur. This is further supported by our observations showing that Rab11a controls TRAM recruitment to phagosomes. Despite the evidence for our model that the ERC is the major source for phagosomal TLR4, it cannot be excluded that also a sequential MyD88- and TRIF-dependent signaling pathway may operate as cell surface TLR4 is internalized during the very early stages of *E. coli* phagocytosis.

The fact that Rab11a is such an important regulator of TLR4 trafficking and IRF3 signaling from *E. coli* phagosome may also be expanded to include LPS-induced IRF3 signaling from endosomes. By comparing *E. coli* particles and LPS, we found that Rab11a silencing also selectively reduced LPS-induced TRAM-TRIF signaling, suggesting that Rab11a also can regulate transport of TLR4 to endosomes.

In summary, we have uncovered an unexpected transport pathway of TLR4 toward the internalized *E. coli* vacuole that involves ERC and Rab11a. This route of TLR4 transport results in the production of IFN-β that takes place from the *E. coli* phagosome. We have found that phagocytosis of Gram-negative bacteria is essential for type I IFN production, which may serve as an important link between the innate and adaptive immune systems in providing host defense against Gram-negative infections.

EXPERIMENTAL PROCEDURES

Reagents and Bacteria

E. coli and *S. aureus* pHrodo Bioparticles (Invitrogen) were used. LPS (0111:B4) from *E. coli* (Invivogen) was Cy5 labeled as previously described (Latz et al., 2002). Cytochalasin D and Brefeldin A1 were purchased from Sigma. DRAQ5 was from Biostatus Limited. Plasmids for bacterial expression of CFP was electroporated into *Y. pestis* KIM5 strains and cultured at 26°C or 37°C to gain bacteria expressing hexaacylated or tetraacylated LPS, respectively (Montminy et al., 2006). Alexa Fluor labeling of Golgin-97 was performed according to the manufacturer's protocol (Invitrogen). The following antibodies were used: mouse-anti-Golgin-97 from Invitrogen; mouse-anti-GAPDH (ab9484) and rabbit-anti-Rab11a (ab3612) from AbCam; rabbit-anti-phos-pho-IRF3 (Ser396), rabbit-anti-total IRF3, and rabbit-anti IkB-α from Cell Signaling; rabbit-anti-TLR4 (H-80), rabbit-anti-Rab7 (H-50), goat-anti-Rab11a (K-15), rabbit-anti-NF-κB p65 (A) antibody, rabbit-anti-IRF3 (FL-425), rabbit-anti-MyD88 (HFL-296), rabbit-anti-TRAM (TICAM-2) (H-85), normal rabbit IgG, and goat IgG from Santa Cruz Biotech. Alexa Fluor labeled secondary antibodies were from Invitrogen. The following mammalian expression vectors were used: pcDNA3.1 (Invitrogen), huCD14, and Elam-luc (Latz et al., 2002); and huMD-2 in pEF-BOS was kindly provided by K. Miyake (University of Tokyo). Rab11aS25N^{GFP} and Rab11aQ70L in pEGFP (Clontech) were kindly provided by M. Zerial (Max Planck Institute of Molecular Cell Biology and Genetics). pGEM-Rab11a was kindly provided by T.G. Iversen (The

Norweigan Radium Hospital, University of Oslo). The Gal4-IRF3 reporter assay was kindly provided by K. Fitzgerald (UMass Med School, Worcester, MA) and T. Maniatis (Harvard University, Cambridge, MA). The ECFP-Rab11a vector was made by inserting the human Rab11a cDNA from pGEM-Rab11a into the $pECFP_{C1}$ vector (Clontech).

Cells

Human monocytes were isolated from buffycoat as previously described (Husebye et al., 2006). Use of human monocytes from blood donors was approved by the Regional Committees from Medical and Health Research Ethics at NTNU. The monocytes were maintained in RPMI1640 (GIBCO) supplemented with 10% or 25% of pooled human A^+ serum (The Blood Bank, St Olavs Hospital, Trondheim, Norway). 25% A^+ serum was used if the incubation time exceeded 24 hr. The HEK293 $TLR4^{Cherry}$ cells were made as previously described (Latz et al., 2002). The HEK293 $TLR4^{YFP}$ and HEK293 $TLR4^{Cherry}$ cells were cultured in DMEM with 10% fetal calf serum (FCS) and 0.5 mg/ml G418 and transfected with GeneJuice transfection reagent (Novagen).

Luciferase Assays

NF-κB activation was determined by the ELAM-luc NF-κB luciferase reporter assay as described (Latz et al., 2002) and IRF3 activation determined with the Gal4-IRF3 assay as described (Fitzgerald et al., 2003). The Renilla luciferase pRL-TK vector (Promega) was cotransfected for normalization.

siRNA Treatment

Monocytes or HEK293 cells were seeded on 35 mm glass-bottom γ-irradiated tissue cell dishes (MatTek Corporation) or 6-well plates (NUNC) at 10×10^6 cells per dish/well containing medium free of antibiotics, before transfection with siRNA via Lipofectamine RNAiMAX transfection reagent (Invitrogen) according to the manufacturer's recommendations. The AllStars Negative Control (QIAGEN) was used as a nonsilencing control RNA and the Hs_RAB11A_5 HP Validated siRNA (QIAGEN) was used to target Rab11a. The cells were treated for 20–72 hr with 20 nM siRNA and, when stated, transfected with indicated plasmid DNA for 24 hr.

Gene Expression Analysis

Gene expression analysis was carried out via QPCR as described in Supplemental Experimental Procedures.

Immunoblotting

Immunoblotting was performed on HEK293 cells expressing $TLR4^{YFP}$ and transfected with MD-2 and CD14 or monocytes as previously described (Husebye et al., 2006). The blots were developed with the SuperSignal West Femto (Thermo Scientific) and visualized with the Image Estimation 2000R (Kodak). For quantification the Kodak 1D Image Analysis software was used.

Confocal Laser Scanning Microscopy

Images of live cells were captured at 37°C with a Zeiss LSM 510 META scanning unit, a heating stage, and a 1.4 NA × 63 objective. For intracellular staining, the cells were fixed with 2% paraformaldehyde in PBS, put 15 min on ice, permeabilized with PEM buffer (80 mM K-Pipes [pH 6.8], 5 mM EGTA, 1 mM $MgCl_2$, 0.05% saponin) for 15 min on ice, quenched of free aldehyde groups in 50 mM NH_4Cl with 0.05% saponin for 5 min, and blocked in PBS with 20% human serum and 0.05% saponin (monocytes) or in PBS with 10% FCS and 0.05% saponin (HEK293 cells) for 20 min. The cells were incubated with primary antibody 2 μg/ml (polyclonal antibodies) or 10 μg/ml (monoclonal antibodies) in PBS with 1% human serum and 0.05% saponin (monocytes) overnight at 4°C or PBS with 0.05% saponin (HEK293 cells) for 60 min at room temperature. Alexa Fluor-labeled secondary antibodies (Invitrogen) were incubated 15 min at room temperature after three washes in PBS with 0.05% saponin.

Quantification of Relative Amounts of Fluorescently Labeled Proteins in Intracellular Compartments

3D data were captured with identical settings and avoiding saturation of voxels (3D pixels) intensities. The ImarisXT software (Bitplane) was used to surface render the imaged structures giving one surface for each ERC. The pHrodo or DRAQ5 fluorescence was used to spot or surface render the volume of individual phagosomes or nuclei, respectively. The software produced a numerical value of the relative amount of TLR4, Rab11a, IRF3, or p65 as a sum of voxel intensities from the original image in each compartment. The values for voxel intensities did not follow a Gaussian distribution, and therefore we used median as a measure of average intensities and the nonparametric Mann-Whitney test to evaluate statistical significance.

Supplementary Material

Refer to Web version on PubMed Central for supplementary material.

ACKNOWLEDGMENTS

This work was supported by grants from the Norwegian Research Council and the Norwegian Cancer Society. The imaging experiments have been performed with equipment and expertise located at the NORMic subcellular imaging nodes in Trondheim and in Oslo.

REFERENCES

Cox D, Lee DJ, Dale BM, Calafat J, and Greenberg S. (2000). A Rab11-containing rapidly recycling compartment in macrophages that promotes phagocytosis. Proc. Natl. Acad. Sci. USA 97, 680–685. [PubMed: 10639139]

Espevik T, Latz E, Lien E, Monks B, and Golenbock DT (2003). Cell distributions and functions of Toll-like receptor 4 studied by fluorescent gene constructs. Scand. J. Infect. Dis 35, 660–664.

Fitzgerald KA, Rowe DC, Barnes BJ, Caffrey DR, Visintin A, Latz E, Monks B, Pitha PM, and Golenbock DT (2003). LPS-TLR4 signaling to IRF-3/7 and NF-kappaB involves the toll adapters TRAM and TRIF. J. Exp. Med 198, 1043–1055. [PubMed: 14517278]

Flannagan RS, Cosío G, and Grinstein S. (2009). Antimicrobial mechanisms of phagocytes and bacterial evasion strategies. Nat. Rev. Microbiol 7, 355–366. [PubMed: 19369951]

Gioannini TL, Teghanemt A, Zhang D, Coussens NP, Dockstader W, Ramaswamy S, and Weiss JP (2004). Isolation of an endotoxin-MD-2 complex that produces Toll-like receptor 4-dependent cell activation at picomolar concentrations. Proc. Natl. Acad. Sci. USA 101, 4186–4191. [PubMed: 15010525]

Goldenring JR, Shen KR, Vaughan HD, and Modlin IM (1993). Identification of a small GTP-binding protein, Rab25, expressed in the gastrointestinal mucosa, kidney, and lung. J. Biol. Chem 268, 18419–18422. [PubMed: 8360141]

Halaas O, Husebye H, and Espevik T. (2007). The journey of Toll-like receptors in the cell. Adv. Exp. Med. Biol 598, 35–48. [PubMed: 17892203]

Hornef MW, Frisan T, Vandewalle A, Normark S, and Richter-Dahlfors A. (2002). Toll-like receptor 4 resides in the Golgi apparatus and colocalizes with internalized lipopolysaccharide in intestinal epithelial cells. J. Exp. Med 195, 559–570. [PubMed: 11877479]

Husebye H, Halaas O, Stenmark H, Tunheim G, Sandanger O, Bogen B, Brech A, Latz E, and Espevik T. (2006). Endocytic pathways regulate Toll-like receptor 4 signaling and link innate and adaptive immunity. EMBO J. 25, 683–692. [PubMed: 16467847]

Ip WKE, Takahashi K, Moore KJ, Stuart LM, and Ezekowitz RAB (2008). Mannose-binding lectin enhances Toll-like receptors 2 and 6 signaling from the phagosome. J. Exp. Med 205, 169–181. [PubMed: 18180310]

Ip WK, Sokolovska A, Charriere GM, Boyer L, Dejardin S, Cappillino MP, Yantosca LM, Takahashi K, Moore KJ, Lacy-Hulbert A, and Stuart LM (2010). Phagocytosis and phagosome acidification are required for pathogen processing and MyD88-dependent responses to Staphylococcus aureus. J. Immunol 184, 7071–7081. [PubMed: 20483752]

Jain V, Halle A, Halmen KA, Lien E, Charrel-Dennis M, Ram S, Golenbock DT, and Visintin A. (2008). Phagocytosis and intracellular killing of MD-2 opsonized gram-negative bacteria depend on TLR4 signaling. Blood 111, 4637–4645. [PubMed: 18203953]

Johnston RB Jr., Klemperer MR, Alper CA, and Rosen FS (1969). The enhancement of bacterial phagocytosis by serum. The role of complement components and two cofactors. J. Exp. Med 129, 1275–1290. [PubMed: 4181833]

Jones MC, Caswell PT, and Norman JC (2006). Endocytic recycling pathways: Emerging regulators of cell migration. Curr. Opin. Cell Biol 18, 549–557. [PubMed: 16904305]

Jordens I, Marsman M, Kuijl C, and Neefjes J. (2005). Rab proteins, connecting transport and vesicle fusion. Traffic 6, 1070–1077. [PubMed: 16262719]

Kagan JC, and Medzhitov R. (2006). Phosphoinositide-mediated adaptor recruitment controls Toll-like receptor signaling. Cell 125, 943–955. [PubMed: 16751103]

Kagan JC, Su T, Horng T, Chow A, Akira S, and Medzhitov R. (2008). TRAM couples endocytosis of Toll-like receptor 4 to the induction of interferon-beta. Nat. Immunol 9, 361–368. [PubMed: 18297073]

Kinchen JM, and Ravichandran KS (2008). Phagosome maturation: Going through the acid test. Nat. Rev. Mol. Cell Biol 9, 781–795. [PubMed: 18813294]

Kobayashi M, Saitoh S, Tanimura N, Takahashi K, Kawasaki K, Nishijima M, Fujimoto Y, Fukase K, Akashi-Takamura S, and Miyake K. (2006). Regulatory roles for MD-2 and TLR4 in ligand-induced receptor clustering. J. Immunol 176, 6211–6218. [PubMed: 16670331]

Lapierre LA, Dorn MC, Zimmerman CF, Navarre J, Burnette JO, and Goldenring JR (2003). Rab11b resides in a vesicular compartment distinct from Rab11a in parietal cells and other epithelial cells. Exp. Cell Res 290, 322–331. [PubMed: 14567990]

Latz E, Visintin A, Lien E, Fitzgerald KA, Monks BG, Kurt-Jones EA, Golenbock DT, and Espevik T. (2002). Lipopolysaccharide rapidly traffics to and from the Golgi apparatus with the toll-like receptor 4-MD-2-CD14 complex in a process that is distinct from the initiation of signal transduction. J. Biol. Chem 277, 47834–47843. [PubMed: 12324469]

Misaki R, Nakagawa T, Fukuda M, Taniguchi N, and Taguchi T. (2007). Spatial segregation of degradation- and recycling-trafficking pathways in COS-1 cells. Biochem. Biophys. Res. Commun 360, 580–585. [PubMed: 17606221]

Montminy SW, Khan N, McGrath S, Walkowicz MJ, Sharp F, Conlon JE, Fukase K, Kusumoto S, Sweet C, Miyake K, et al. (2006). Virulence factors of Yersinia pestis are overcome by a strong lipopolysaccharide response. Nat. Immunol 7, 1066–1073. [PubMed: 16980981]

Murray RZ, Kay JG, Sangermani DG, and Stow JL (2005). A role for the phagosome in cytokine secretion. Science 310, 1492–1495. [PubMed: 16282525]

Nilsen N, Nonstad U, Khan N, Knetter CF, Akira S, Sundan A, Espevik T, and Lien E. (2004). Lipopolysaccharide and double-stranded RNA upregulate toll-like receptor 2 independently of myeloid differentiation factor 88. J. Biol. Chem 279, 39727–39735. [PubMed: 15190057]

O'Neill LA, and Bowie AG (2007). The family of five: TIR-domain-containing adaptors in Toll-like receptor signalling. Nat. Rev. Immunol 7, 353–364. [PubMed: 17457343]

Ozinsky A, Underhill DM, Fontenot JD, Hajjar AM, Smith KD, Wilson CB, Schroeder L, and Aderem A. (2000). The repertoire for pattern recognition of pathogens by the innate immune system is defined by cooperation between toll-like receptors. Proc. Natl. Acad. Sci. USA 97, 13766–13771. [PubMed: 11095740]

Parent A, Hamelin E, Germain P, and Parent JL (2009). Rab11 regulates the recycling of the beta2-adrenergic receptor through a direct interaction. Biochem. J 418, 163–172. [PubMed: 18983266]

Poltorak A, He X, Smirnova I, Liu MY, Van Huffel C, Du X, Birdwell D, Alejos E, Silva M, Galanos C, et al. (1998). Defective LPS signaling in C3H/ HeJ and C57BL/10ScCr mice: mutations in Tlr4 gene. Science 282, 2085–2088. [PubMed: 9851930]

Saraste J, and Goud B. (2007). Functional symmetry of endomembranes. Mol. Biol. Cell 18, 1430–1436. [PubMed: 17267686]

Tissiè res P, Dunn-Siegrist I, Schä ppi M, Elson G, Comte R, Nobre V, and Pugin J. (2008). Soluble MD-2 is an acute-phase protein and an opsonin for Gram-negative bacteria. Blood 111, 2122–2131. [PubMed: 18056837]

Ullrich O, Reinsch S, Urbé S, Zerial M, and Parton RG (1996). Rab11 regulates recycling through the pericentriolar recycling endosome. J. Cell Biol 135, 913–924. [PubMed: 8922376]

Uronen-Hansson H, Allen J, Osman M, Squires G, Klein N, and Callard RE (2004). Toll-like receptor 2 (TLR2) and TLR4 are present inside human dendritic cells, associated with microtubules and the Golgi apparatus but are not detectable on the cell surface: Integrity of microtubules is required for interleukin-12 production in response to internalized bacteria. Immunology 111, 173–178. [PubMed: 15027902]

Waage A, Brandtzaeg P, Halstensen A, Kierulf P, and Espevik T. (1989). The complex pattern of cytokines in serum from patients with meningococcal septic shock. Association between interleukin 6, interleukin 1, and fatal outcome. J. Exp. Med 169, 333–338. [PubMed: 2783334]

Wei J, Liu Y, Bose K, Henry GD, and Baleja JD (2009). Disorder and structure in the Rab11 binding domain of Rab11 family interacting protein 2. Biochemistry 48, 549–557. [PubMed: 19119858]

Zerial M, and McBride H. (2001). Rab proteins as membrane organizers. Nat. Rev. Mol. Cell Biol 2, 107–117. [PubMed: 11252952]

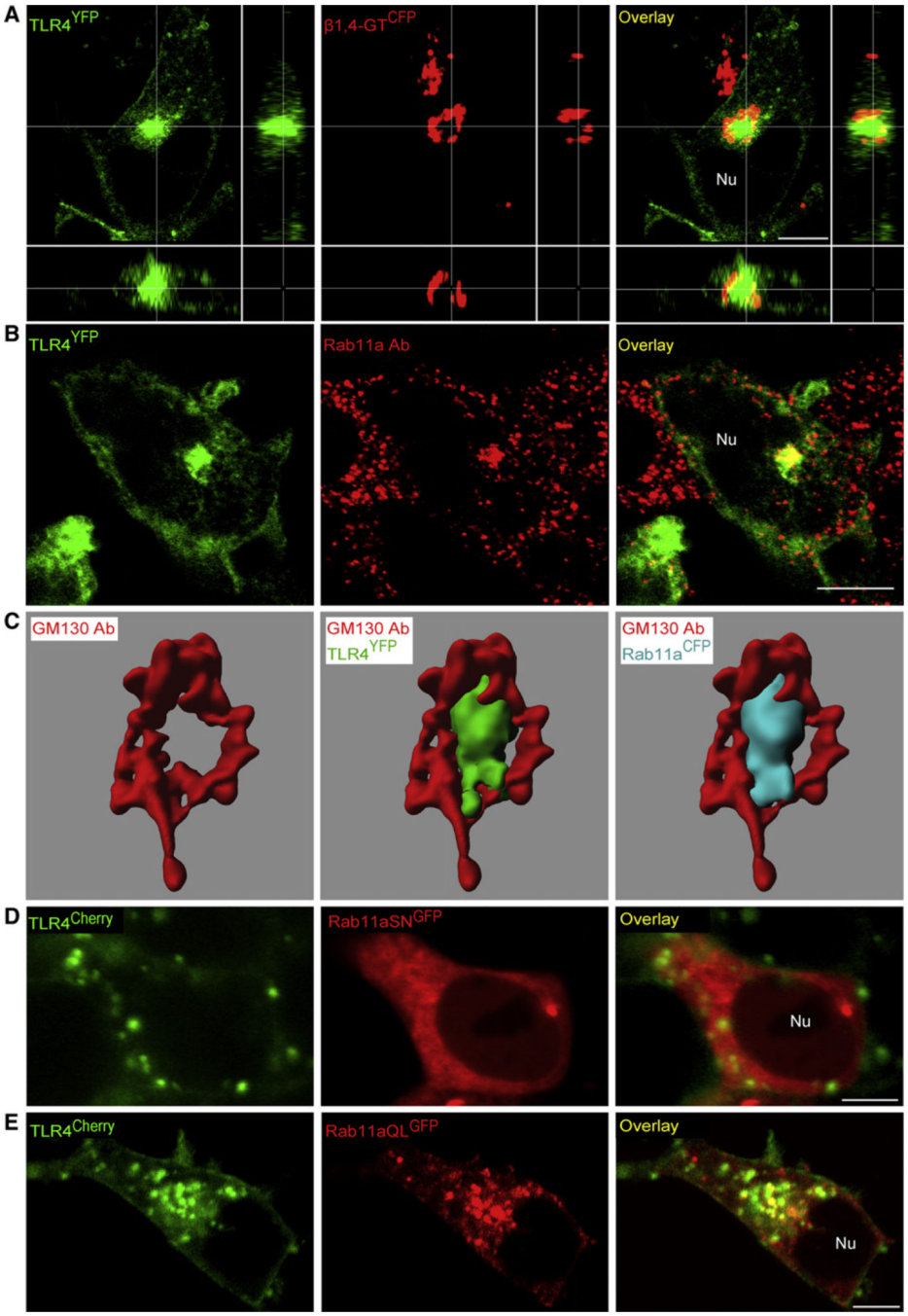

Figure 1. The Rab11a-Positive ERC Contains High Amounts of TLR4 in HEK293 TLR4^{YFP} Cells

Orthographic and planar projection data were obtained via confocal microscopy on fixed cells. Overlapping regions appear as yellow in the overlay panels.

(A) Orthographic projections of HEK293-TLR4^{YFP} cells coexpressing the trans-medial Golgi marker β−1,4 galactosyl transferase linked to CFP (β−1,4 GT^{CFP}).

(B) Planar sections of HEK293-TLR4^{YFP} cells stained for endogenous Rab11a via the Rab11a antibody (ab3612).

(C) 3D modeling of the cis-Golgi (GM130), TLR4^{YFP}, and Rab11a^{CFP} in HEK293-TLR4^{YFP} cells cotransfected with Rab11a^{CFP}, MD-2, and CD14.
(D and E) HEK-TLR4^{Cherry} cells cotransfected with dominant-negative GDP-bound Rab11aSN^{GFP} (D) or constitutive active GTP-bound Rab11aQL^{GFP} (E) together with MD-2 and CD14.
Scale bars represent 10 μm. Data are representative of four independent experiments. See also Figure S1.

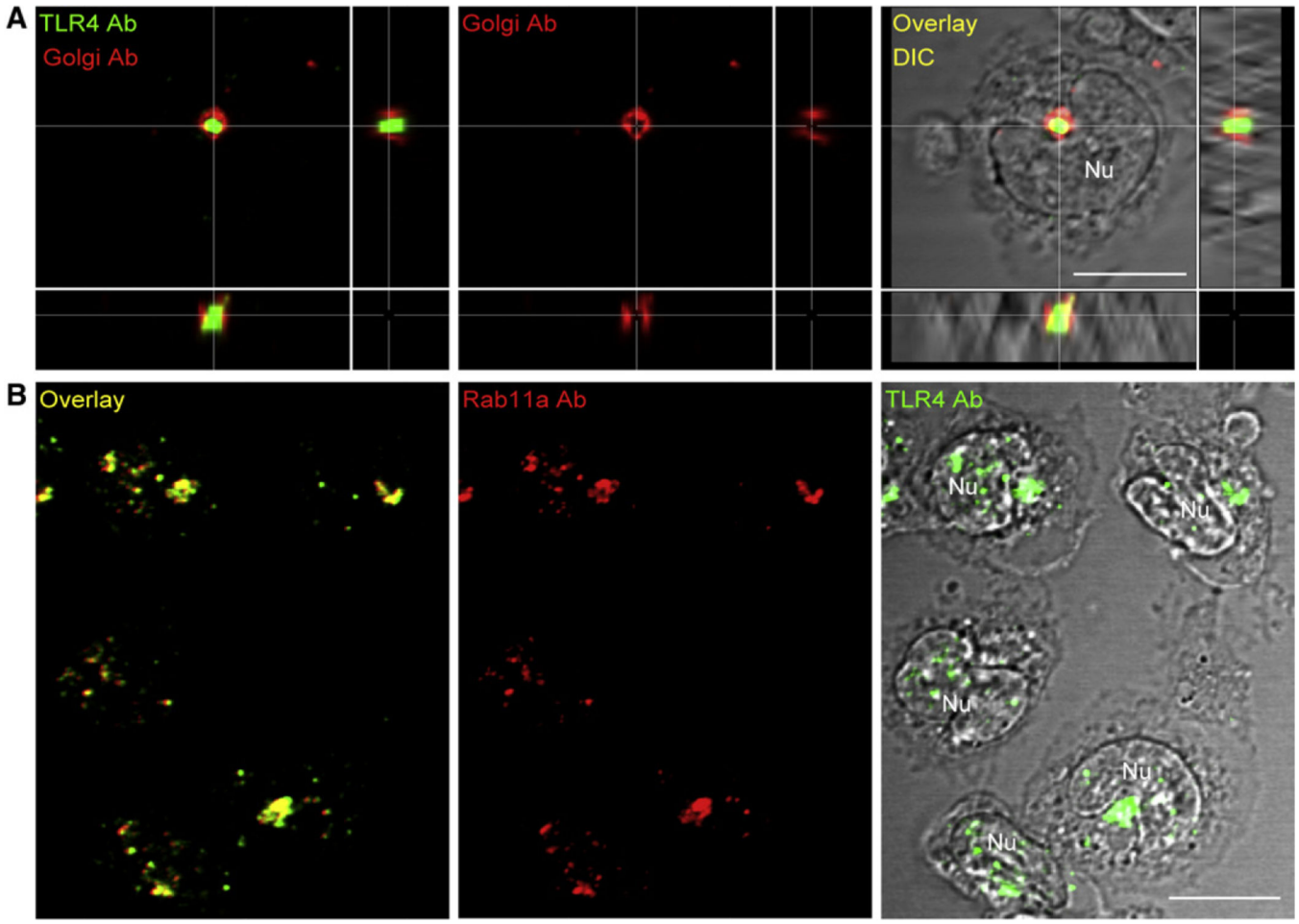

Figure 2. The Rab11a-Positive ERC Contains High Amounts of TLR4 in Human Monocytes

Orthographic and planar projection data were obtained with confocal microscopy on fixed cells. Overlapping regions appear as yellow in the overlay panels.

(A) Orthographic projections of a human monocyte costained for TLR4 and trans-medial Golgi (Golgin-97).

(B) Human monocytes costained for TLR4 and Rab11a.

Scale bars represent 10 μm. Data are representative of three independent experiments. See also Figure S2.

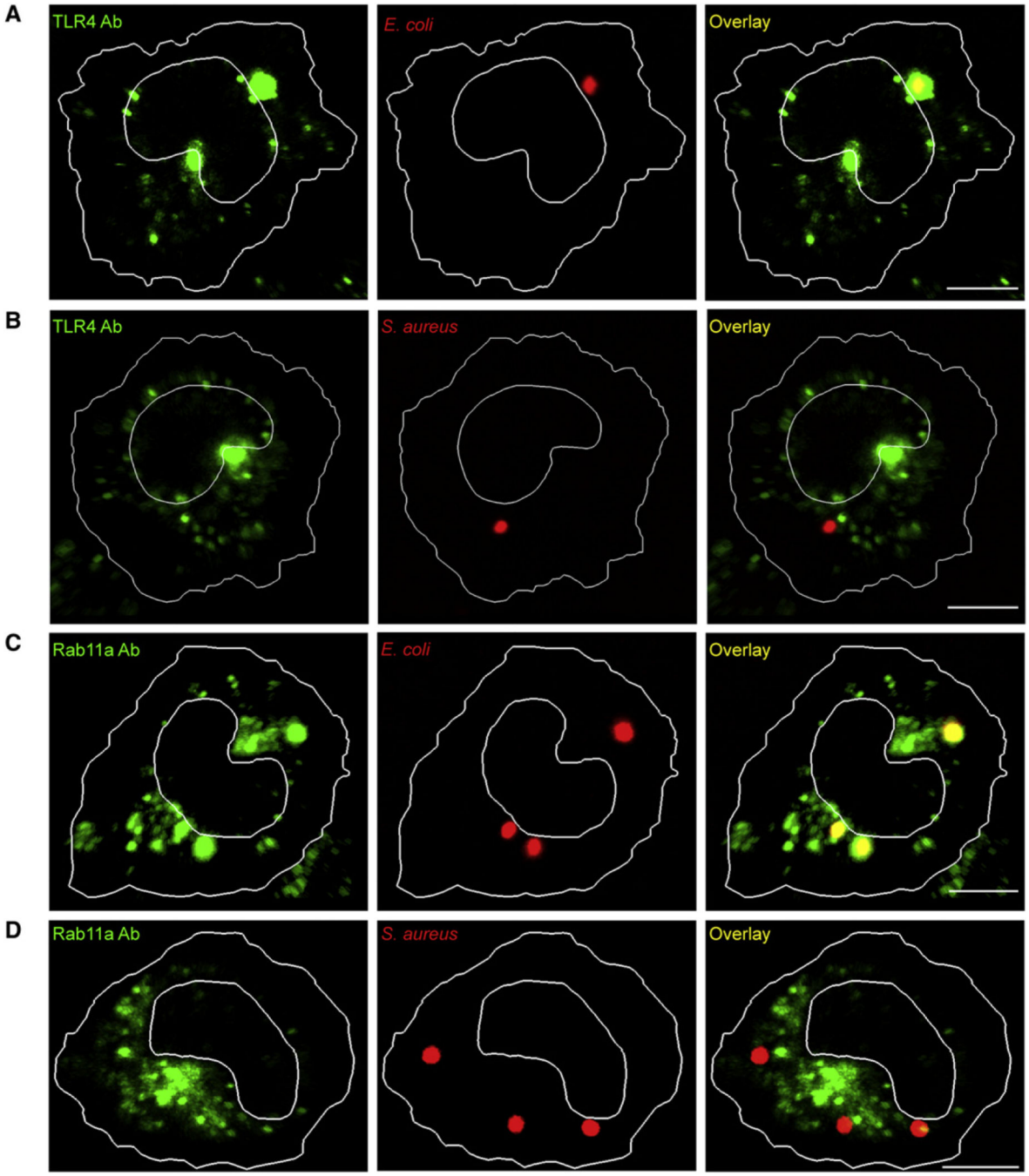

Figure 3. TLR4 and Rab11a Accumulate around Phagocytosed *E. coli*, but Not around *S. aureus*

Human monocytes were incubated with *E. coli* or *S. aureus* particles (5.0×10^6/ml) for 15 min and fixed and stained for TLR4 or Rab11a. Overlapping regions appear as yellow in the overlay panels.

(A) TLR4 accumulates toward the *E. coli* phagosome. TLR4 (green), *E. coli* (red), and overlay (right).

(B) TLR4 does not accumulate toward the *S. aureus* phagosome. TLR4 (green), *S. aureus* (red), and overlay (right).

(C) Rab11a accumulates toward the *E. coli* phagosome. Rab11a (green), *E. coli* (red), and overlay (right).
(D) Rab11a does not accumulate toward the *S. aureus* phagosome. Rab11a (green), *S. aureus* (red), and overlay (right).
Scale bars represent 10 μm. Data are representative of three independent experiments. See also Figure S3.

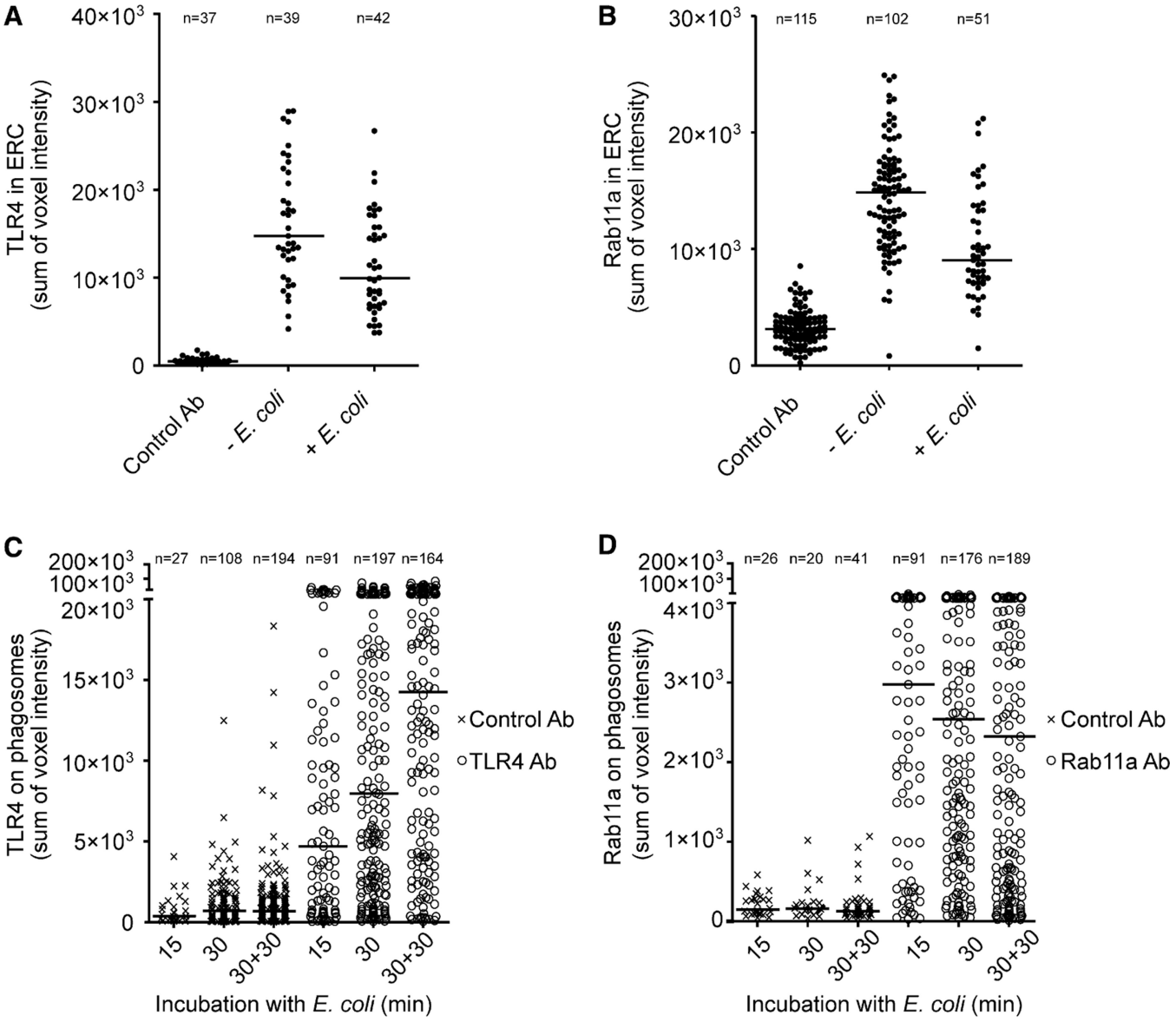

Figure 4. Addition of *E. coli* to Human Monocytes Results in Intracellular Redistribution of TLR4 and Rab11a

Human monocytes were incubated with *E. coli* particels (2×10^6/ml), fixed, and immunostained for TLR4 or Rab11a.

(A) TLR4 voxel intensity in the ERC in cells incubated with or without *E. coli* for 15 min was measured ($p = 0.001$).

(B) Rab11a voxel intensity in the ERC in cells incubated with or without *E. coli* for 15 min ($p < 0.0001$).

(C) TLR4 voxel intensity on *E. coli* phagosomes as a function of incubation time ($p < 0.0001$ for TLR4 from 15 min to 30+30 min).

(D) Rab11a voxel intensity on *E. coli* phagosomes as a function of incubation time ($p = 0.046$ for Rab11a from 15 min to 30+30 min).

Bars in plots represent the median. n = number of observations. Data are representative of three independent experiments. See also Figure S4 and Movie S1.

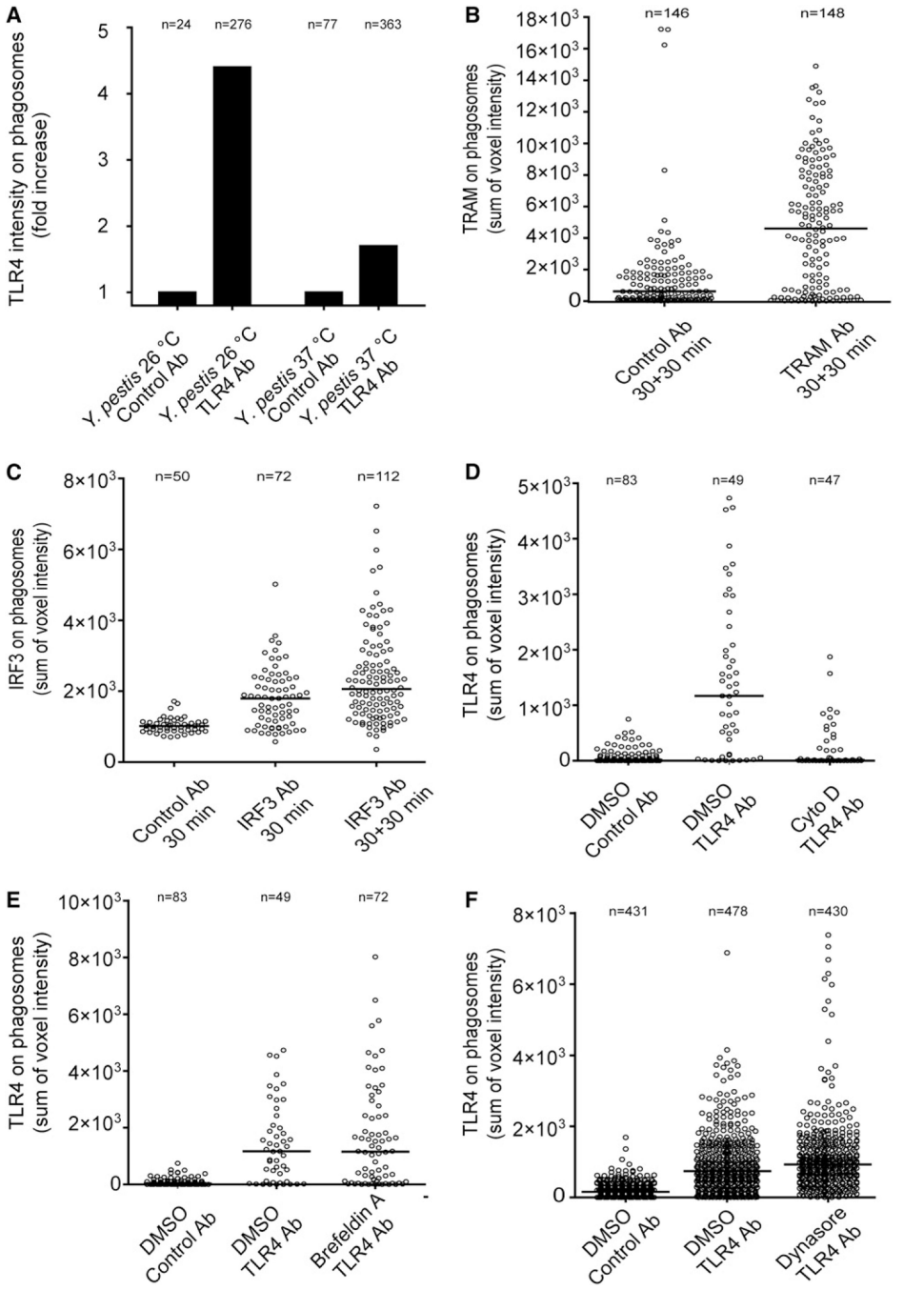

Figure 5. Recruitment of TLR4 to *E. coli* Phagosomes Requires TLR4 Signaling and Intact Actin Filaments, but Not Dynamin

Human monocytes incubated with bacterial particles, fixed, and immunostained for TLR4, TRAM, and MyD88; with normal rabbit IgG as control antibody.

(A) TLR4 recruitment to the phagosome requires TLR4 signaling. Fold increase in phagosomal TLR4 voxel intensity in cells immunostained for TLR4 versus cells stained with control antibody. Cells were incubated 30 min with heat-killed *Y. pestis* (2×10^6/ml) cultured at 26°C or 37°C.

(B) TRAM voxel intensity on *E. coli* phagosomes ($p < 0.0001$).

(C) IRF3 voxel intensity on *E. coli* phagosomes. An increase in IRF3 was observed from 30 min to 30+30 min ($p < 0.0028$).
(D) TLR4 recruitment to *E. coli* phagosomes requires intact actin filaments. Cells were pretreated with 2 μM cytochalasin D (cyto D) or vehicle (DMSO) for 30 min and incubated with *E. coli* for 30 min in the presence of inhibitor or vehicle ($p < 0.0001$).
(E) TLR4 recruitment to *E. coli* phagosomes occurs independent of Golgi. The cells were pretreated with 5 μg/ml Brefeldin A or vehicle (DMSO) and incubated 30 min with *E. coli* in the presence of inhibitor or vehicle.
(F) Inhibition of dynamin does not cause a reduction in phagosomal TLR4. Monocytes were incubated for 2 hr under serum-free conditions and treated for 30 min with opsonized *E. coli.* Subsequently the cells were washed two times and incubated for 30 min with 80 μM Dynasore or vehicle (DMSO) in serum-free medium ($p = 0.0002$ for DMSO and Dynasore treatments).
Monocytes were incubated with *E. coli* particles ($3.0–8.0 \times 10^6$/ml) (B–F).
Bars in plots represent the median. n = number of observations. Data are representative of three independent experiments. See also Figure S5.

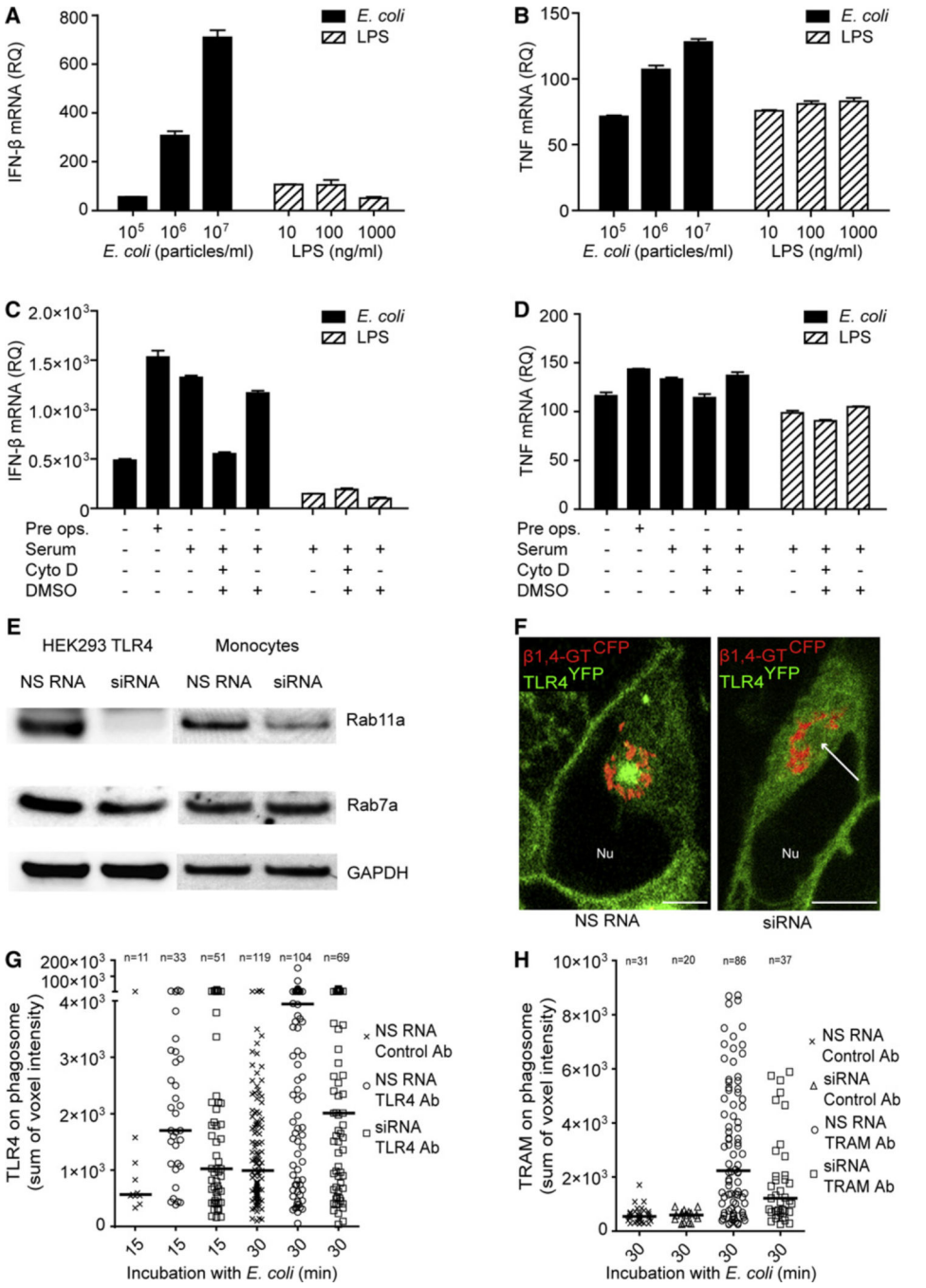

Figure 6. *E. coli*-Induced IFN-β Signaling Requires Phagocytosis, and TLR4 Recruitment to Phagosomes Is Rab11a Dependent

(A and B) Induction of IFN-β mRNA (A) and TNF mRNA (B) in monocytes stimulated for 60 min with different concentrations of *E. coli* particles or LPS. The amounts of IFN-β and TNF mRNAs were determined by QPCR and is presented as mean relative to nonstimulated monocytes and standard deviations.

(C and D) Induction of IFN-β (C) and TNF mRNAs (D) in monocytes stimulated with *E. coli* particles (8.0×10^6/ml) or LPS (100 ng/ml) for 60 min. The impact of phagocytosis was examined by incubation with or without human A+ serum, with or without preopsonization

as well as the phagocytosis inhibitor Cyto D or vehicle (DMSO). The amounts of IFN-β and TNF mRNAs were determined by QPCR and are presented as mean relative to nonstimulated monocytes and standard deviations.

(E) HEK293-TLR4^{YFP} cells or human monocytes were treated with nonsilencing RNA oligo (NS RNA) or Rab11a siRNA, cellular lysates were made, and immunoblotting performed with Rab11a antibody (ab3612) or Rab7a antibody. GAPDH was used for control of equal loading.

(F) Confocal image of TLR4^{YFP} (green) in HEK293-TLR4^{YFP} cells coexpressing β−1,4 GT^{CFP} (red) treated with NS RNA (left) or Rab11a siRNA (right). The arrow indicates the center of the Golgi ring.

(G) TLR4 on *E. coli* phagosomes in monocytes treated with NS RNA or Rab11a siRNA and stimulated with *E. coli* particles (3×10^6/ml), p = 0.05 and p = 0.03 for TLR4 amounts in NS RNA compared to Rab11a siRNA-treated cells at 15 min and 30 min, respectively.

(H) TRAM on *E. coli* phagosomes in monocytes treated with NS RNA or Rab11a siRNA stimulated with *E. coli* particles (3×10^6/ml), p = 0.02 for TRAM amounts in NS RNA-compared to siRNA-treated cells.

Bars in plots represent the median. n = number observations. Data are representative of four independent experiments. Scale bars represent 5 μm. See also Figure S6.

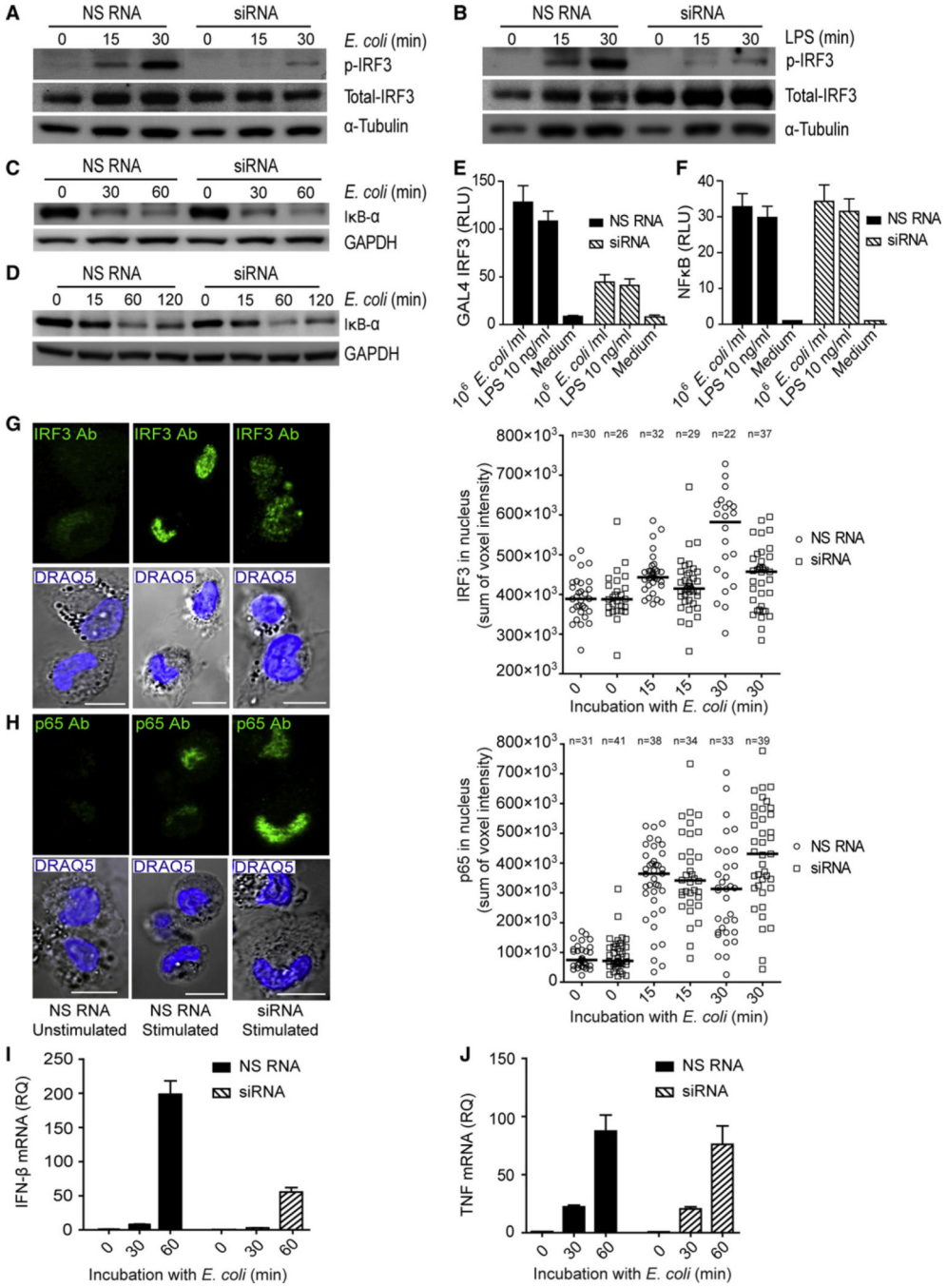

Figure 7. Silencing of Rab11a Selectively Affects TLR4-Mediated IRF3 Activation and IFN-β Induction

(A and B) Human monocytes were treated with NS RNA or siRNA (48 hr) and stimulated with *E. coli* particles (A) or LPS (B) as indicated. Immunoblotting was performed with IRF3 antibodies recognizing phosphorylated-IRF3 (Ser 396) and total-IRF3. α-Tubulin was used as a control of equal loading.

(C and D) IkB-α degradation in siRNA-treated monocytes (C) and HEK293TLR4^{YFP} cells (D) stimulated with *E. coli* particles (1.0×10^7/ml) as indicated, with GAPDH as loading control.

(E and F) HEK293 TLR4^{Cherry} cells treated with siRNA or NS RNA for 72 hr, plated, and transfected with MD-2, CD14, and the Gal4-IRF3-luciferase reporter (E) or the NF-κB-luciferase reporter (F). The cells were incubated with *E. coli* or LPS for 9 hr. Gal4-IRF3 activation was normalized toward Renilla Luciferase. Activation is presented as mean relative luciferase units (RLU) to Gal4DBD signals and standard deviations.

(G and H) Human monocytes treated with NS RNA or siRNA and stimulated with *E. coli* (3.0×10^6/ml) as indicated, fixed, and immunostained for total IRF3 (G) or total p65 (H). Quantification of nuclear IRF3 (G). Silencing of Rab11a resulted in decreased nuclear IRF3 translocation compared to NS RNA-treated cells (15 min; $p = 0.0145$, 30 min; $p = 0.0009$). Quantification of nuclear p65 (H). Silencing of Rab11a resulted in increased nuclear p65 translocation at 30 min ($p = 0.0031$). Bars represent the median. n = number of observations. Scale bars represent 10 μm.

(I and J) Human monocytes treated with NS RNA or siRNA for 20 hr were stimulated with *E. coli* particles (3.0×10^6/ml) as indicated. Total RNA was isolated and the level of IFN-β and TNF mRNA quantified by QPCR shown as mean relative to reference sample (NS RNA, 0 min) and standard deviations. Data are representative of three independent experiments. See also Figure S7.